Cold electron and ion beams generated from trapped atoms

Cold electron and ion beams generated from trapped atoms

B. J. Claessens, M. P. Reijnders, G. Taban, O. J. Luiten, and E. J. D. Vredenbregt[a)]
Center for Plasma Physics and Radiation Technology, Department of Applied Physics, Eindhoven University of Technology, P.O. Box 513, 5600 MB Eindhoven, The Netherlands

(Received 4 June 2007; accepted 24 July 2007; published online 5 September 2007)

A novel way of creating low-temperature electron and ion beams is demonstrated. The beams are generated by converting a laser-cooled atom cloud to a highly excited Rydberg gas, which subsequently develops into an ultracold plasma. Charged particles are extracted from the Rydberg gas and the plasma by a pulsed electric field. The properties of the resulting electron and ion pulses are experimentally studied. Pulses of a few hundred ns duration containing a few pC of charge were observed. Upper limits for the temperature of such beams (60 K for ions and 500 K for electrons) are obtained, and the beams are shown to have low emittance. Further development of the method may lead to the generation of high-brightness charged-particle beams from ultracold plasmas.
 [DOI: 10.1063/1.2771518]

I. INTRODUCTION

In a recent publication,[1] we argued that ultracold plasmas (UCPs) (Refs. 2–4) may provide an entirely new way of generating high-brightness charged-particle beams. Such plasmas, which are created by near-threshold ionization of a cloud of laser-cooled atoms, provide a unique medium with ion and electron temperatures in the 1 mK and 10 K range, respectively. These temperatures are orders of magnitude lower than the 10^4 K (1 eV) that is typical for electron and ion beams generated by field-emission[5,6] and photoemission[7] sources. A low temperature T is beneficial for the intrinsic brightness B of a source since $B \propto I/(AT)$, where I is the current and A is the cross-sectional area of the source. Therefore, UCP-based ion and electron sources offer an alternative route to improving brightness compared to the development of needle sources[5] and carbon nanotube (CNT) emitters,[6] which aim at reducing the area A.

The continued interest in ion and electron source development stems from their ubiquitous use in a wide range of research areas such as materials science, chemistry, and biology, as well as in industry. Focused ion beams (FIBs),[8] for example, provide nanoscale milling and imaging capabilities to the semiconductor industry, while secondary ion mass spectrometry (SIMS) (Ref. 9) is used to analyze the protein distribution in biological cells,[10] among others. Using electrons, so-called laser synchrotrons[11] generate ultrashort pulses of x-rays by nonlinear Thomson scattering, while ultrafast electron microscopes (UEMs) (Refs. 12 and 13) provide a dynamical view of physical and chemical processes with picosecond and nanometer resolution. However, further advances, such as achieving the holy grail in the field of UEM, i.e., single-shot images and diffraction patterns, or focused ion beam milling on the 1 nm scale, and achieving useful output from laser synchrotrons, depend on the development of charged particle sources with brightness beyond the current state-of-the-art.[11,13]

Here we report an experimental investigation of the properties of both ion and electron beams extracted from ultracold plasmas and Rydberg atoms. While ions and electrons have been extracted from ultracold plasmas before,[3,4] so far this was done as a diagnostic of the plasma. Here, instead, we focus on the properties of the extracted particles themselves, with applications such as ultrafast electron diffraction and focused ion beams in mind. We show that such beams indeed have low temperatures (with upper limits of 60 K for ions and 500 K for electrons), and, as a result, low emittance and high angular intensity. These measurements thus demonstrate the potential of the method we proposed in our earlier publication.[1] At the same time, we find that achieving state-of-the-art brightness requires further experimental advances.

II. EXPERIMENTAL ROUTINE AND SETUP

To generate an UCP, we start by collecting a sample of $\approx 10^8$ laser-cooled ^{85}Rb atoms in a vapor-cell magneto-optical atom trap (MOT).[14] The root-mean-square (rms) size of the cloud is 1 mm and the central density is 6×10^9 atoms/cm^3. Around 45% of the atoms are in the upper level of the $5s\ ^2S_{1/2}(F=3) \leftrightarrow 5p\ ^2P_{3/2}(F=4)$ transition that the trapping laser excites. The magnetic field necessary for trapping can be turned off within 50 μs.

To create the plasma, the trapped atoms are illuminated by the output of a pulsed dye laser that is tuned to the transition from the $5p\ ^2P_{3/2}$ level to the $44d\ ^2D$ Rydberg state (wavelength 480 nm).[15] The 6 ns long laser pulses contain 1 mJ of energy in a several mm wide beam. We estimate the resulting density of Rydberg atoms at 10^9 atoms/cm^3, enough for the cloud to spontaneously develop into a plasma on a time scale of a few μs.[4]

The MOT is surrounded by an acceleration structure consisting of four 16 cm long rods separated by 20 mm (see Fig. 1). A voltage pulse with a risetime of 1 μs and variable amplitude $V_m = 0-800$ V can be applied to the bottom two rods, while the top two rods are held at ground potential. This provides a pulsed electric field at the center of the rod structure that can reach a maximum value of 300 V/cm and

[a)]Electronic mail: E.J.D.Vredenbregt@tue.nl

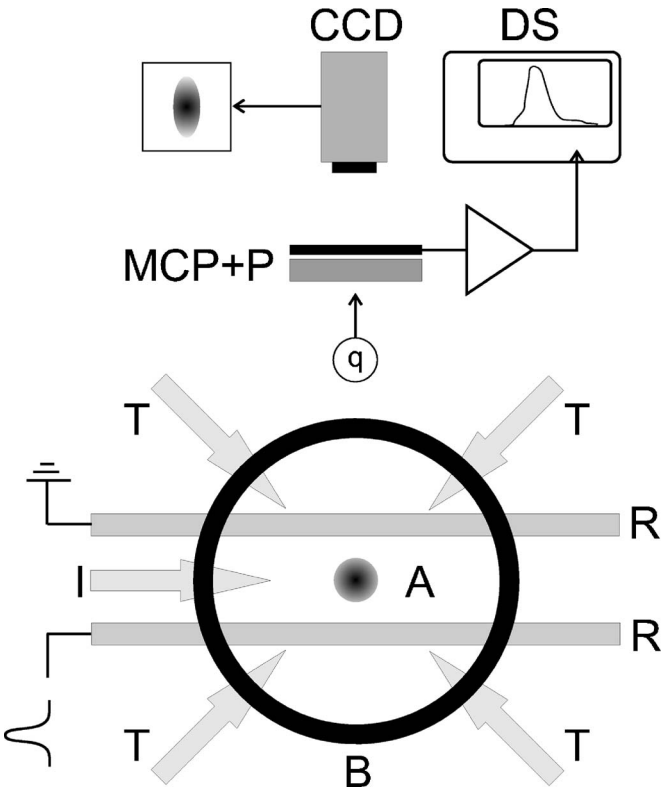

FIG. 1. Schematic view of the setup, showing atom cloud (A), trapping laser beams (T), magnetic field coils (B), ionization laser beam (I), accelerating rods (R), MCP plus phosphor assembly (MCP+P), digital oscilloscope (DS), and camera (CCD).

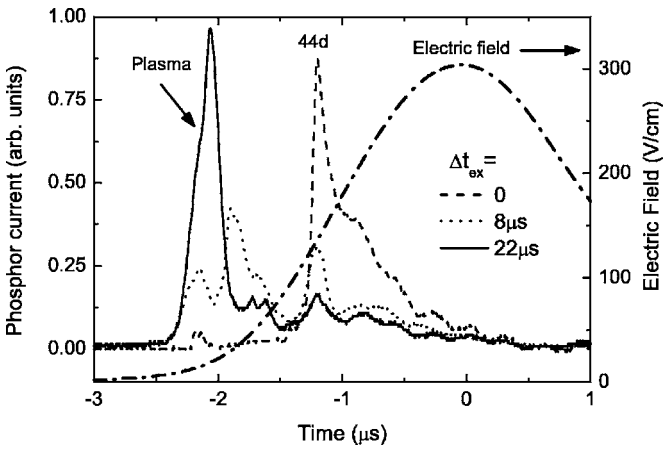

FIG. 2. Electron traces: current (left scale) detected on phosphor versus time when electrons are accelerated toward the MCP assembly, for various values of delay time Δt_{ex} between ionization laser pulse and extraction pulse. The dashed-dotted line shows the extraction field (right scale).

is constant within 10% over a distance of 4 mm. The field pulse is used to extract either ions or electrons from the plasma (depending on the polarity of the pulse) and to accelerate them toward a microchannel plate (MCP) plus phosphor assembly located a distance $L=22$ cm above the MOT. In addition, the pulse field-ionizes any remaining Rydberg atoms, which also results in a signal on the MCP.

The MCP serves to amplify the incident charge, which is then accelerated toward the phosphor screen, where it creates an image representing the time-integrated, spatial charge distribution of the arriving ion or electron pulse. The image is recorded with a charge-coupled device (CCD) camera. At the same time, the time dependence of the amplified charge that reaches the phosphor screen can be measured with a digital oscilloscope via a fast transimpedance amplifier. A metal grid in front of the MCP assembly ensures that it does not disturb the electric field at the position of the MOT. The operating conditions of the MCP assembly were such that it operated in a linear charge amplification regime. The gain of the MCP was set to 100 for electrons and to 10^4 for ions during the experiments, with an uncertainty of a factor of 2. The charges reported below have all been corrected for MCP gain. The quantum efficiency of the MCP is unknown, however; in what follows we will assume it to be unity so that we always report a lower limit on the observed charge.

In the experiment, after allowing the number of atoms in the MOT to reach a steady state, both the magnetic field and the trapping laser are suddenly turned off. Following a delay of 100 μs in which the magnetic field is allowed to die out, the trapping lasers are turned back on to populate the $5p$ level. Another 20 μs later, the dye laser pulse arrives and creates a cloud of cold Rydberg atoms. Then, after a variable delay of $\Delta t_{ex}=0-80$ μs, the extraction field is pulsed on. The resulting charge pulse is recorded on the oscilloscope while the CCD camera records the image visible on the phosphor screen. The whole sequence is then repeated at the 10 Hz repetition rate of the pulsed laser.

III. EXPERIMENTAL RESULTS

Figure 2 shows the time-dependence of the electron signal recorded on the oscilloscope in such experiments, for various values of the delay time Δt_{ex} between the dye laser pulse and the extraction pulse. The origin of the horizontal axis coincides with the maximum of the extraction pulse; the pulse shape is also shown in the figure. For no delay ($\Delta t_{ex}=0$ μs in Fig. 2), we only observe a signal due to field-ionization of the Rb $44d$ Rydberg state excited by the pulsed laser. For intermediate delay times ($\Delta t_{ex}=8$ μs), the signal extends to both earlier and later times, signifying a redistribution of Rydberg atoms over states with both higher and lower principle quantum number n, due to interactions with electrons.[16] Finally, at even longer delay times ($\Delta t_{ex}=22$ μs), a large peak appears at very low electric field that corresponds to weakly bound electrons, consistent with the formation of an UCP. This peak corresponds to a 1.2 pC electron pulse with a rms width of 200 ns and a peak current of 2.3 μA.

Analogous results are obtained when the polarity of the extraction pulse is reversed, so that ions rather than electrons are pushed toward the MCP assembly. For $\Delta t_{ex}=22$ μs delay, we detect a 0.3 pC ion pulse with a rms width of 800 ns and a peak current of 0.16 μA. The main difference with the electron signals is a much larger flight time t_f of the ions ($t_f=11.5$ μs compared to $t_f\approx 60$ ns for electrons), due to their larger mass.

The inset of Fig. 3 shows an image of an ion pulse (lower panel) and of an electron pulse (upper panel) as re-

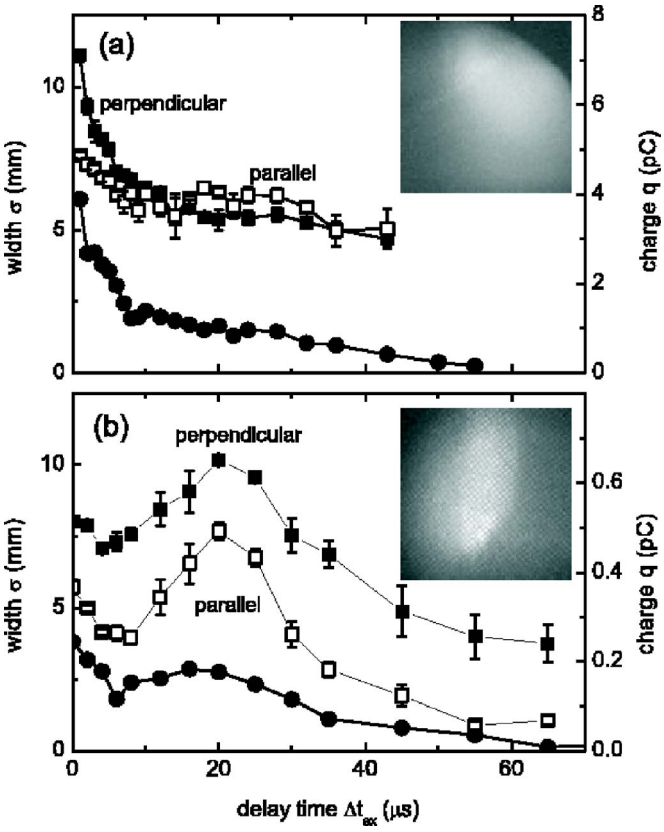

FIG. 3. (Color online) Measured spatial width σ (left axis) of electron (panel a) and ion (panel b) images versus delay time Δt_{ex} in parallel (open squares) and perpendicular (solid squares) direction. Also shown is the corresponding total extracted charge q (solid circles; right axis). The insets show actual recorded images (size 25×25 mm).

corded by the CCD camera. To characterize the spatial distribution of these pulses, we fit them to a two-dimensional Gaussian distribution. The extracted rms widths σ in the directions parallel and perpendicular to the rods (indicated in Fig. 1), are plotted versus delay time Δt_{ex} in Fig. 3.

For the ions, the width recorded in the perpendicular direction is always larger than in the parallel direction. This can be attributed to a difference in "exit kick," meaning that the accelerating rod structure acts on the ion cloud as a negative lens with a greater strength in the perpendicular than in the parallel direction. The negative lens effect occurs because the electric field in the z-direction decreases going from the center of the rod structure toward the MCP detector, requiring a gradient in the fields in the parallel and perpendicular directions since the divergence $\vec{\nabla}\cdot\vec{E}$ of the electric field $\vec{E}$ must vanish. Due to the geometry of the rod structure, with the length of the bars several times their distance to the center, the gradient in the electric field is greater in the perpendicular than in the parallel direction, leading to the experimentally observed difference in widths.

In both directions, the widths first decrease for small Δt_{ex}, then rise to a maximum before attaining a finite asymptotic value for large Δt_{ex}. The reason for this behavior is that the width is influenced by the amount of charge that is liberated, since space charge forces will result in additional expansion of a bunch.[17] To show the importance of this effect, the figure also shows the total charge q arriving on the MCP, derived by integrating the signal in ion traces, equivalent to those shown in Fig. 2 for electrons, which were simultaneously recorded with the images. The collected charge shows similar behavior as the widths, implying that the divergence of the beam is space-charge dominated. The decay of the charge at small Δt_{ex} is due to the formation of Rydberg atoms with low principal quantum number ($n\lesssim35$) which are not field-ionized in our experiment, resulting from spontaneous decay and n-mixing collisions.[16,18] When a plasma forms, many of these low-lying states are ionized, leading to the maximum in the charge curve near $\Delta t_{ex}=20$ μs. Obviously, the maximum in the charge curve coincides with the maximum in the width curve.

Figure 3 also shows equivalent curves in the case that the polarity of the extraction voltage is chosen such that electrons instead of ions are accelerated toward the MCP assembly. Here the exit kick and the maximum in width and charge are less apparent. This is at least partially due to stray magnetic fields, since fields of 1 Gauss already give rise to cyclotron motion with a period on the order of $1/t_f$. This causes a mixing of the parallel and perpendicular degrees of freedom, as well as reduced detection efficiency for weakly bound, plasma electrons. These gain appreciably less kinetic energy ($\approx$30 eV) from the field than electrons generated by field-ionization of 44d Rydberg atoms so that their trajectories undergo greater deflection. As a result, the total recorded charge decays with increasing Δt_{ex}, while the recorded widths in parallel and perpendicular direction are almost the same, except for small Δt_{ex}, where all electrons have high energy.

IV. ANALYSIS

In Fig. 4 we plot the width of the images as a function of the collected charge for both ion and electron pulses. Here the correlation between width and charge of the pulse can be clearly observed, not only for ions but also for electrons.

Included in the figure is a set of curves resulting from particle-tracking simulations using the GPT computer code.[19] In these simulations, a cloud of charged particles is followed in time from the moment of creation near the center of the rod structure until the MCP is reached, in the mean time undergoing external electrical forces stemming from the rod structure as well as internal space-charge forces. The spatial distribution of the electric field generated by the combination of the rods and the vacuum enclosure was calculated with the SUPERFISH Poisson solver, and its temporal shape modeled by the measured acceleration pulse shown in Fig. 2. Uncertainties in these calculations include the position of the particles with respect to the center of the rod structure at the moment of ionization, as well as the precise time of creation of a particle since, according to Fig. 2, the Rydberg atoms are distributed over a range of states that will field-ionize at different fields. For electrons, for which the flight time to the detector ($<$100 ns) is less than the temporal width of the observed signals, this stretches out the length of the bunch substantially in a way that is difficult to model quantitatively. In turn, this dilution of the charge density in the bunch sub-

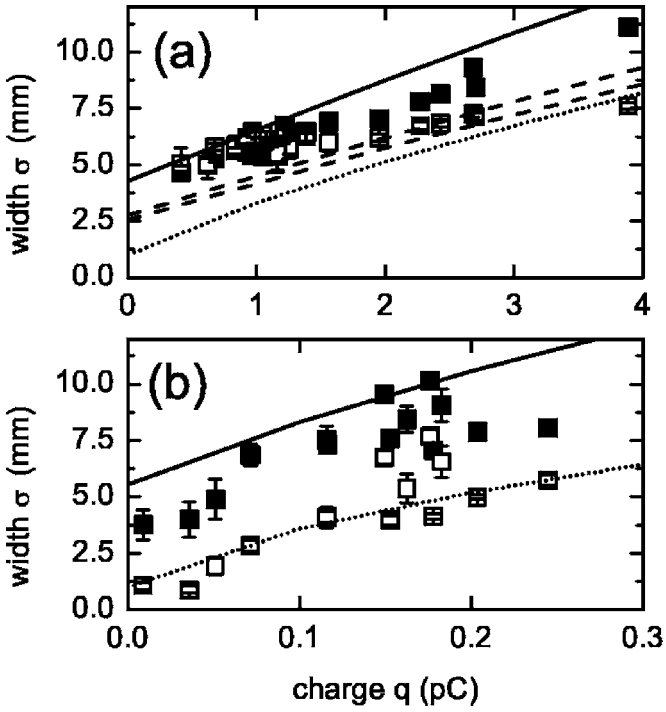

FIG. 4. Measured spatial width of electron (panel a) and ion (panel b) images versus extracted charge. Solid (open) squares: perpendicular (parallel) direction. The solid (dotted) lines represent perpendicular (parallel) widths calculated with particle tracking simulations described in the text; for the dashed lines a 2 G homogeneous magnetic field is added.

stantially reduces the transverse expansion of the electron bunch, which the present simulations therefore cannot predict with any certainty. For ions, however, this effect plays a very minor role due to the larger mass.

The bottom panel of Fig. 4 shows that for the ions the simulations match the data quite well. In particular, the difference in widths for the parallel and perpendicular direction, and the increase of the widths with the charge of the liberated ion cloud are fairly well reproduced. In these simulations the initial distribution of the ions was taken to be Gaussian with a rms width of 1 mm and the initial temperature taken to be zero. The agreement confirms that the divergence of the ion beam is dominated by space-charge forces rather than ballistic expansion related to the temperature of the particles, and that the perpendicular width is increased by the "exit kick" effect.

The top panel of Fig. 4 shows that, to a lesser degree, space charge forces also influence the divergence of the electron beam. Here also, the essential features of the experimental data can be reproduced by simulations. If the initial temporal length of the (electron) charge cloud is taken to be around 75 ns, the simulations (represented by the solid and dotted lines in the figure) approximately match the observed slope of width *v* charge (solid and dotted lines in the figure). If, in addition, a constant magnetic field of ≈ 2 Gauss pointing in the *z*-direction is assumed, the perpendicular and parallel widths of the electron cloud are effectively mixed up (dashed lines), as is observed in the experiment. As shown in the figure, the simulations also predict that if the magnetic field could be properly nulled, the parallel width of the electron beam would also fall well below 2 mm at zero charge, since the exit kick depends mostly on the properties of the electric field and thus should be about the same for electrons and ions.

We can obtain an upper limit on the transverse temperature T of the ion and electron beams from the widths σ_0 observed for the lowest charge ($\sigma_0 = 0.9 \pm 0.2$ mm for ions and $\sigma_0 = 5.0 \pm 0.5$ mm for electrons) if we know the time of flight t_f by setting $kT = m(\sigma_0/t_f)^2$, where m is the mass of an electron or Rb^+ ion and k is Boltzmann's constant. For the ion signals, $t_f = 11.5 \pm 1.0$ μs can be determined from the observed time dependence of the signals, leading to $T = 60 \pm 30$ K. For the electrons, we use the computed $t_f = 60 \pm 25$ ns giving $T = 500 \pm 400$ K.

The derived electron temperature is appreciably higher than the $T \approx 25$ K found for direct UCP creation,[20] again pointing to the role of stray fields. Nevertheless, a source temperature of 500 K is one to two orders of magnitude lower than reported for needle sources,[5] CNTs,[6] and photoguns,[7] signifying a major advance. The temperature derived for ions is also larger than expected for ultracold plasmas ($T \approx 1$ K, Ref. 21). Here, this is due to the fact that the size of the plasma, which is around 1 mm and thus comparable to σ_0, is neglected in our estimate because we do not know the size of the source accurately enough to correct for it; the actual temperature will therefore be appreciably lower. Even so, the derived ion temperature is already three orders of magnitude lower than the 5×10^4 K (4.5 eV) reported for the liquid-metal ion (LMI) source.

V. DISCUSSION

The measured widths σ and the measured peak currents I_p, together with the estimated initial rms size $\sigma_i = 1$ mm can be combined in various ways to derive figures of merit for the extracted beams. For nonrelativistic beams, commonly used quantities are the reduced emittance $\epsilon_r = \sigma_i \alpha \sqrt{E}$, reduced angular intensity $(dI/d\Omega)_r = I_p/(\Omega E)$ and reduced brightness $B_r = I_p/(A\Omega E) = I_p/(4\pi^2 \epsilon_r^2)$. Here, $A = 2\pi\sigma_i^2$ is the source area, $\Omega = 2\pi\alpha^2$ is the solid angle subtended by the beam with $\alpha = \sigma/L$ the corresponding half-angle, and $E = (1/2)m(L/t_f)^2$ is the average longitudinal kinetic energy. Alternative, "normalized" quantities ϵ_n and B_n (used for relativistic electron beams) can be deduced from the given "reduced" quantities by replacing E by $2E/mc^2$ where c is the speed of light. In Table I we have collected the values for these quantities, as derived from the numbers for σ, σ_i, I_p, and t_f quoted above, together with values that may be considered state-of-the-art.

The comparison in the table points out the wide variety encountered in charged-particle sources. According to the table, the electron and ion beams studied in this paper outperform existing pulsed electron sources (photoguns) and continuous ion sources (the LMI) in terms of emittance. This is due precisely to the low temperature available only from UCPs, the basic premise of the idea expressed in Ref. 1. Electron beams derived from CNTs have even much lower emittance, but these are limited to low (100 nA) current. Also, the angular intensity of the cold, pulsed ion beam is appreciably higher than the LMI provides. On the other

TABLE I. Summary of beam parameters.

	ϵ_r (ϵ_n) mm mrad $\sqrt{\text{eV}}$ (mm mrad)	$(dI/d\Omega)_r$ nA/sr eV	B_r (B_n) A/m^2 sr eV (A/m^2 sr)
electron sources:			
this work	140 (0.3)	$2\ 10^4$	$2\ (6\times10^{-6})$
CNTs[a]	$0.003\ (6\times10^{-6})$	3	10^9 (4000)
photoguns[b]	400 (0.8)	6×10^{10}	10^7 (40)
ion sources:			
this work	50	10^4	3
LMI[c]	1000	5	10^6

[a]Reference 6.
[b]Reference 7.
[c]References 8 and 22.

hand, it also follows from the table that the brightness of the cold beams studied here as reported in the table is not yet compatible with the state-of-the-art.

In part, this is caused by the limitations of the experiment: we expect the actual temperatures of the beams to be appreciably lower than the limits we have been able to set so far, implying appreciably higher brightness than listed in Table I. Apart from that, there are two distinct routes toward higher brightness. For the pulsed electron source, increasing the beam energy through a higher slew rate of the accelerating field produces higher current at the same charge and thus higher brightness.[1] In this case, the brightness of the beams is further increased by the velocity bunching effect described in Ref. 1. For the ion source, reducing the temperature towards the 0.1 mK of the trapped atoms by operating it in a continuous mode, increases its brightness toward that of the LMI at low operating current while allowing for a smaller longitudinal energy spread.[23] Further brightness gains are possible by increasing the density of the trapped atoms, accompanied by shaping the initial charge cloud to reduce the detrimental effect of space charge.[17] Such advances should allow UCP-based sources to reach the full potential pointed out in Refs. 1, 23, and 24.

To summarize, we have experimentally demonstrated the generation of electron and ion beams from ultracold plasmas and Rydberg gases. Measurements of their spatial and temporal distribution show that such beams are indeed much colder than state-of-the-art charged particle sources can provide. As a result, they have low emittance and high angular intensity. Achieving higher brightness requires further optimization of measurement techniques, and of trapping, ionization and acceleration conditions, which are presently under development in our laboratory.

ACKNOWLEDGMENTS

We thank B. van der Geer, R. Wijtvliet, E. van Kempen, K. Hendriks, and D. Kusters for contributions to this work, and L. van Moll, J. van de Ven, A. Kemper, and H. van Doorn for technical assistance. We also acknowledge helpful discussions with R. Scholten and T. Gallagher, and thank R. van de Sanden for the loan of the pulsed dye laser.

This work is part of the research programme of the "Stichting voor Fundamenteel Onderzoek der Materie (FOM)," which is financially supported by the "Nederlandse Organisatie voor Wetenschappelijk Onderzoek (NWO)."

[1] B. J. Claessens, S. B. van der Geer, G. Taban, E. J. D. Vredenbregt, and O. J. Luiten, Phys. Rev. Lett. **95**, 164801 (2005).
[2] T. C. Killian, Science **316**, 705 (2007).
[3] T. C. Killian, S. Kulin, S. D. Bergeson, L. A. Orozco, C. Orzel, and S. L. Rolston, Phys. Rev. Lett. **83**, 4776 (1999).
[4] M. P. Robinson, B. Laburthe Tolra, M. W. Noel, T. F. Gallagher, and P. Pillet, Phys. Rev. Lett. **85**, 4466 (2000).
[5] C. H. Garcia and C. A. Brau, Nucl. Instrum. Methods Phys. Res. A **483**, 273 (2002).
[6] N. de Jonge, M. Allioux, J. T. Oostveen, K. B. K. Teo, and W. I. Milne, Phys. Rev. Lett. **94**, 186807 (2005).
[7] See P. Piot, in *The Physics and Applications of High Brightness Electron Beams*, edited by J. Rosenzweig, G. Travish, and L. Serafini (World Scientific, Singapore, 2003), p. 127.
[8] J. Orloff, M. Utlaut, and L. Swanson, *High Resolution Focused Ion Beams*, (Kluwer Academic, New York, 2003).
[9] L. Van Vaeck, A. Adriaens, and R. Gijbels, Mass Spectrom. Rev. **18**, 1 (1999).
[10] R. M. A. Heeren, Proteomics **5**, 4316 (2005).
[11] Y. Y. Lau, F. He, D. P. Umstadter, and R. Kowalczyck, Phys. Plasmas **10**, 2155 (2003).
[12] A. H. Zewail, Philos. Trans. R. Soc. London, Ser. A **364**, 315 (2005); V. A. Lobastov, R. Shrinivasan, and A. H. Zewail, Proc. Natl. Acad. Sci. U.S.A. **102**, 7069 (2005).
[13] W. E. King, G. H. Campbell, A. M. Frank, B. W. Reed, J. Schmerge, B. J. Siwick, B. C. Stuart, and P. M. Weber, J. Appl. Phys. **97**, 111101 (2005).
[14] H. J. Metcalf and P. van der Straten, *Laser Cooling and Trapping* (Springer, Berlin, 1999), p. 156.
[15] For an overview of the properties of Rydberg atoms, see T. F. Gallagher, *Rydberg Atoms* (Cambridge University Press, Cambridge, 1994).
[16] A. Walz-Flannigan, J. R. Guest, J.-H. Choi, and G. Raithel, Phys. Rev. A **69**, 063405 (2004).
[17] O. J. Luiten, S. B. van der Geer, M. J. de Loos, F. B. Kiewiet, and M. J. van der Wiel, Phys. Rev. Lett. **93**, 094802 (2004).
[18] A. L. de Oliveira, M. W. Mancini, V. S. Bagnato, and L. G. Marcassa, Phys. Rev. A **65**, 031401(R) (2002).
[19] B. van der Geer and M. J. de Loos, "The general particle tracer code: Design, implementation and application," Ph.D. thesis, Technische Universiteit Eindhoven, Eindhoven (2001).
[20] J. L. Roberts, C. D. Fertig, M. J. Lim, and S. L. Rolston, Phys. Rev. Lett. **92**, 253003 (2004).
[21] Y. C. Chen, C. E. Simien, S. Laha, P. Gupta, Y. N. Martinez, P. G. Mickelson, S. B. Nagel, and T. C. Killian, Phys. Rev. Lett. **93**, 265003 (2004).
[22] G. D. Alton and P. M. Read, J. Phys. D **22**, 1029 (1989); To be in accord with our definition, the emittance value included in Table I is 0.25× the value in their Fig. 7 interpolated for 47% fractional current.
[23] S. B. van der Geer, M. P. Reijnders, P. H. A. Mutsaers, E. J. D. Vredenbregt, and O. J. Luiten, "Simulated performance of an ultracold ion source" (to be published).
[24] J. L. Hanssen, J. J. McClelland, E. A. Dakin, and M. Jacka, Phys. Rev. A **74**, 063416 (2006).